

## Optimizing tip-surface interactions in ESR-STM experiments

S. A. Rodríguez<sup>1</sup>, S. S. Gómez<sup>1</sup>, J. Fernández-Rossier<sup>2,\*</sup> and A. Ferrón<sup>1,†</sup>

<sup>1</sup>*Instituto de Modelado e Innovación Tecnológica (CONICET-UNNE) and Facultad de Ciencias Exactas, Naturales y Agrimensura, Universidad Nacional del Nordeste, Avenida Libertad 5400, W3404AAS Corrientes, Argentina*

<sup>2</sup>*International Iberian Nanotechnology Laboratory (INL), Av. Mestre José Veiga, 4715-330 Braga, Portugal*

 (Received 31 December 2022; revised 16 March 2023; accepted 27 March 2023; published 7 April 2023)

Electron-spin resonance carried out with scanning tunneling microscopes (ESR-STM) is a recently developed experimental technique that is attracting enormous interest on account of its potential to carry out single-spin on-surface resonance with subatomic resolution. Here we carry out a theoretical study of the role of tip-adatom interactions and provide guidelines for choosing the experimental parameters in order to optimize spin resonance measurements. We consider the case of the Fe adatom on a MgO surface and its interaction with the spin-polarized STM tip. We address three problems: first, how to optimize the tip-sample distance to cancel the effective magnetic field created by the tip on the surface spin, in order to carry out proper magnetic field sensing. Second, how to reduce the voltage dependence of the surface-spin resonance frequency, in order to minimize tip-induced decoherence due to voltage noise. Third, we propose an experimental protocol to infer the detuning angle between the applied field and the tip magnetization, which plays a crucial role in the modeling of the experimental results.

DOI: [10.1103/PhysRevB.107.155406](https://doi.org/10.1103/PhysRevB.107.155406)

### I. INTRODUCTION

Properly designed experiments seek to minimize the influence of the probing apparatus on the system of interest. This becomes increasingly difficult at the nanoscale, where macroscopic instruments interact with nanometric systems, and particularly challenging when it comes to probe quantum systems. In this work, we address this issue in the context of electron spin resonance (ESR) driven with a scanning tunneling microscope (STM). After several decades of attempts [1,2], reproducible ESR-STM of individual adatoms on a surface of MgO(100)/Ag was reported in 2015 [3]. This has paved the way for many other outstanding advances in the study of spin physics of individual magnetic atoms [4–13]. Spin resonance of isolated magnetic atoms promises novel applications ranging from quantum information technology to atomic-scale magnetometry.

ESR-STM has now been implemented in several different labs, extending the temperature range, both down to the milli-Kelvin regime [14,15], as well as towards higher temperatures [16,17]. Recently experiments with higher driving frequencies were performed [18]. ESR-STM has been demonstrated now in individual atoms (Fe, Cu), hydrogenated Ti [6,10,15,19], both alone and in artificially created structures such as dimers [6,9,19,20], trimers, and tetramers [21], and on alkali atoms on MgO [22], as well as molecules [23,24]. The state-of-the-art spectral resolution of this ESR-STM, down to a few MHz, makes it possible to resolve the hyperfine structure of Fe, Ti,

and Cu atoms [8,10,25]. ESR-STM setup can also be used to manipulate surface spins coherently [26], with pulses, as well as to drive nuclear spin states [10].

Different mechanisms can account for the driving of the surface spin by the tip bias voltage [2,27–33]. For instance, in Ref. [29], two of us proposed a mechanism based on the modulation of the exchange interaction between the magnetic tip and the magnetic adatom, that originates from the piezoelectric distortion of the adatom. In Ref. [32], we proposed another complementary mechanism, that can coexist with the others, based on the electric modulation of the  $g$  tensor associated with the piezoelectric distortion of the adatom.

Spin interactions between the tip and on-surface species are definitely needed for the detection of ESR-STM, as the resonance readout is magnetoresistive, but they also bring unwanted features, such as uncontrolled variations of the local magnetic field of the surface spins that make absolute magnetometry measurements difficult and may also induce dephasing on the surface spin as mechanical and electrical noise leads to spin noise. Expectedly, the magnetic interaction between the tip and the surface spins strongly depends on their separation, the nature of the ad-atom, the tip design, and the angle formed by the tip magnetization vector and the applied field, which is nonzero on account of the tip magnetic anisotropy [12,29,34]. Importantly, the tip-atom distance is expected to depend on the DC voltage drop at the STM-surface junction, on account of the piezoelectric displacement of the surface spins [29,35]. Therefore we see the tip exerts an influence on the surface spins.

The main goal of the present work is to provide a theoretical basis that permits to control and quantify this influence, thereby improving the sensing capabilities of ESR-STM. Specifically, we consider the case of a single Fe atom on MgO

\*On leave from Departamento de Física Aplicada, Universidad de Alicante, 03690 Spain.

†Corresponding author: [aferron@exa.unne.edu.ar](mailto:aferron@exa.unne.edu.ar)

and address three problems: First, we analyze the optimal tip-adatom distance that minimizes the tip-induced effective magnetic field on the surface spin. This point is known as the No-tip influence (NOTIN) point  $z_n$  and it was described by Seifert and co-workers in Ref. [34] as the sweet spot where the tip does not influence the measured resonance frequency. Second, we study how to reduce the voltage dependence of the surface-spin resonance frequency and we show how this reduces tip-induced decoherence due to voltage noise. Third, we propose an experimental protocol to infer the detuning angle  $\eta$  between the applied field and the tip magnetization, which plays a crucial role in modeling the experimental results.

The rest of this paper is organized as follows. In Sec. II, we present our models to address the problem of ESR-STM experiments in Fe at MgO. Section III is devoted to the study of the resonance frequency and the effect of the tip in ESR-STM experiments. We analyze, in detail, the possibility of optimizing the tip-sample interaction to perform ESR-STM experiments. In Sec. IV, we propose a simple method to determine the main magnetic properties of the STM tip. Finally in Sec. V, we describe the most important findings and summarize the conclusions of the work.

## II. MODEL HAMILTONIAN

### A. Spin Hamiltonian

The spin physics of individual adatoms can be described at two different levels [36]. First, a multiorbital electronic model for the outermost  $d$  electrons, which includes Coulomb interactions, crystal field, and spin-orbit coupling, which we describe in Appendix A. The ground state manifold, obtained by numerical diagonalization, can be also described with an effective *spin model*. For the case of Fe on MgO, the effective spin model, at zero field and ignoring coupling to the tip, is given by [3,32,37,38]

$$\hat{H}_{\text{eff}} = -\mathcal{D}_2 \hat{S}_z^2 + \mathcal{D}_4 \hat{S}_z^4 - \mathcal{F} (\hat{S}_+^4 + \hat{S}_-^4), \quad (1)$$

where the spin operators act on the  $S = 2$  subspace. The anisotropy terms  $\mathcal{D}_2$ ,  $\mathcal{D}_4$ , and  $\mathcal{F}$  can be obtained from the diagonalization of the multiorbital electronic model (MoEM) as shown in Appendix B. Now, the spectrum of the ground state manifold has an ESR active space formed by a doublet of states with  $S_z = \pm 2$ . Yet, this doublet has a zero-field splitting (ZFS), given by  $\Delta_{\text{ZFS}} = 48\mathcal{F} = 0.2 \mu\text{eV}$ , due to quantum spin tunneling [39–41]. We treat tip spin as a classical unit vector  $\hat{n}_T$ . As a result, the interaction of the adatom with the tip can be treated as an effective field:

$$\mathcal{H}_1 = \mu_B \sum_{\beta=x,y,z} g^\beta B_{\text{eff}}^\beta S^\beta. \quad (2)$$

If the magnetic field is along the  $z$  direction, we find that the gap between the ground state and the first excited state is

$$\Delta \approx 2\sqrt{(24\mathcal{F})^2 + (2\mu_B g^z B_{\text{eff}}^z)^2}. \quad (3)$$

This equation is still true if we add the component of the magnetic field along the  $x$  direction, as long as the Zeeman energy associated to  $B_{\text{eff}}^x$  is smaller than  $\mathcal{D}_2 + \mathcal{D}_4$ , as we show in Appendix B. In the present case, the effective field  $\vec{B}_{\text{eff}}$  is the sum of three contributions, external magnetic field, dipolar

field of the tip, and exchange field of the tip:

$$B_{\text{eff}}^\beta = B^\beta + \frac{J_{\text{ex}}(z)}{g^\beta \mu_B} n_T^\beta + B_{\text{tip}}^\beta \equiv B^\beta + B_{\text{tip}}^\beta, \quad (4)$$

where  $B^\beta$  is the  $\beta = x, y, z$  component of the external magnetic field,

$$J_{\text{ex}}(z) = \langle S_{\text{tip}} \rangle J_0 e^{-z/l_0} \quad (5)$$

is the distance-dependent tip-adatom exchange,  $S_{\text{tip}}$  is the spin of the tip and  $n_T^\beta$  are the components of the unit vector that describes the orientation of the tip spin. The exchange coupling can be written as in most of the experimental works [12] as  $J_{\text{ex}}(z) = \langle S_{\text{tip}} \rangle J_0^* e^{-(z-z_{pc})/l_0}$  by doing  $J_0 = J_0^* e^{z_{pc}/l_0}$  and  $z_{pc}$  is the tip height above point contact and can be measured for the Fe atom [12] ( $z_{pc} \simeq 0.4 \text{ nm}$ ). Because of its magnetic anisotropy, the tip magnetization can be misaligned from the external field by an angle  $\eta$ :

$$\hat{n}_T = (\cos(\theta + \eta), 0, \sin(\theta + \eta)). \quad (6)$$

Given the  $C_4$  symmetry of the Fe adatom on top of an oxygen atom on the 001 MgO surface, we can assume the external field lies in the  $xz$  plane:

$$\vec{B} = B(\cos \theta, 0, \sin \theta). \quad (7)$$

The dipolar interaction between the magnetic moment of the tip and the surface spin comes from the magnetic field created by the tip [12],

$$\vec{B}_{\text{dip}} = \frac{\mu_0 M_{\text{tip}}}{4\pi |z|^3} (\hat{n}_T - 3(\hat{n}_T \cdot \hat{z}) \cdot \hat{z}), \quad (8)$$

where  $M_{\text{tip}} = \mu_B g_{\text{tip}} N_t \langle S_{\text{tip}} \rangle$ ,  $g_{\text{tip}}$  is the  $g$ -factor of the atoms in the tip,  $N_t$  is the number of Fe atoms in the tip and  $\hat{z}$  and  $\hat{z}$  are the vector and the unit vector from tip to surface atom, respectively. When the Fe atom and the tip are just above the O atom we have  $\vec{B}_{\text{dip}} = \mu_0 M_{\text{tip}} \hat{n}_{\text{dip}} / (4\pi |z|^3)$ , where  $\hat{n}_{\text{dip}} = (\cos(\theta + \eta), 0, -2 \sin(\theta + \eta))$ . In the literature [12], the values of  $M_{\text{tip}} \simeq 10\mu_B - 40\mu_B$  seems to be reasonable.

Altogether, we obtain the following expression for the  $z$  component of the effective field that acts on the Fe adatom:

$$B_{\text{eff}}^{(z)} = \left( \frac{J_{\text{ex}}(z)}{g^z \mu_B} - 2 \frac{\mu_0 M_{\text{tip}}}{4\pi |z|^3} \right) \sin(\theta + \eta) + B \sin \theta \quad (9)$$

In the rest of the work, and so that our results show agreement with some of the last experiments, we will use  $M_{\text{tip}} = 30\mu_B$ ,  $l_0 = 0.04 \text{ nm}$ ,  $J_0^* = 1 \text{ meV}$  ( $J_0 = 20 \text{ eV}$ ), and  $\langle S_{\text{tip}} \rangle = 2$ .

### B. Effect of the tip-electric field on the surface spin

In actual ESR-STM experiments, there is a DC bias, with amplitude  $V_{\text{DC}}$ , superimposed to the AC bias  $V_{\text{RF}} \sin(\omega t)$ . Applying an electric field induces a strain  $\delta z$  of the bond between the Fe adatom and the oxygen atom underneath [29]. This leads to a modulation of the crystal field [29,32] and the magnetic field induced by the tip [29] (see Appendix C). The electric field across the gap between the STM and the Fe atom,  $E = V_{\text{DC}}/d_{\text{tip}}$ , where  $d_{\text{tip}}$  is the tip-atom distance when there is no electric field and  $z = d_{\text{tip}} - \delta z$ , induces a force on the adatom,  $F \simeq qV_{\text{DC}}/d_{\text{tip}}$  on account of its charge  $q$ . This force is compensated by a restoring elastic force  $F = -k\delta z$ . Then,

we can evaluate how much the Fe atom is displaced from its equilibrium position [29]:

$$\delta z \simeq \frac{qV_{\text{DC}}}{kd_{\text{tip}}}. \quad (10)$$

With this sign convention, increasing  $V_{\text{DC}}$  leads to a stretching of the Fe-O bond and a reduction of the tip-Fe distance. In the present case, we have  $q = 2$  and, from DFT calculations for Fe on MgO [29,32], we obtain  $k = 600 \text{ eV nm}^{-2}$ . We find a modulation of the crystal field parameters in the multi-orbital fermionic model (see Appendix A and Appendix C) whose low energy states are described by Eq. (1). Using DFT calculations, we have computed this dependence for Fe on MgO [29,32]. Numerical diagonalization of the multi-orbital model that takes into account the modulation of the crystal field parameters as we described in Appendix C gives

$$\begin{aligned} \mathcal{D}_i &= \mathcal{D}_{i_{\text{eq}}} + \alpha_{\mathcal{D}_i} \delta z, \\ \mathcal{F} &= \mathcal{F}_{\text{eq}} + \alpha_{\mathcal{F}} \delta z, \\ g^\beta &= g_{\text{eq}}^\beta + \alpha_{g^\beta} \delta z, \end{aligned} \quad (11)$$

where the equilibrium parameters are those corresponding to a zero electric field when the piezoelectric displacement is not present. The parameters  $\alpha_X$  are defined and evaluated in Appendix C and account for the effect of the piezoelectric displacement on the atom-surface interaction.

The combination of the piezoelectric distortion of the atom-tip distance due to the external electric field [Eq. (10)] and the crystal field parameter modulation [Eq. (11)] lead also to a modulation of the effective tip-induced field:

$$\frac{\partial B_{\text{eff}}^\beta}{\partial z} = \frac{\partial J_{\text{ex}}(z)}{\partial z} \frac{1}{g^\beta \mu_B} n_T^\beta + \frac{\partial B_{\text{dip}}^\beta}{\partial z} - \frac{J_{\text{exc}}(z)}{(g^\beta)^2 \mu_B} \frac{\partial g^\beta}{\partial z}. \quad (12)$$

Finally, we can express the shift in the adatom resonance frequency,  $f = \Delta/h$ , as follows:

$$\delta f = \frac{\partial f}{\partial B_{\text{eff}}^\beta} \frac{\partial B_{\text{eff}}^\beta}{\partial z} \delta z + \frac{\partial f}{\partial \mathcal{F}} \frac{\partial \mathcal{F}}{\partial z} \delta z + \frac{\partial f}{\partial g^\beta} \frac{\partial g^\beta}{\partial z} \delta z \quad (13)$$

with  $\beta = z$ .

### III. SWEET SPOTS FOR OPTIMAL TIP-SAMPLE INTERACTIONS

We now study how to optimize experimental parameters in the ESR-STM setup, such as the tip-adatom distance  $d_{\text{tip}}$  and the DC voltage  $V_{\text{DC}}$ . Specifically, we devote ourselves to describing two special points of operation. First, the optimal  $d_{\text{tip}}$  for which the effective magnetic field of the tip vanishes. Second, the regions in the  $d_{\text{tip}}, V_{\text{DC}}$  plane where the variation of the frequency with respect to  $V_{\text{DC}}$  is either large, affording voltage-controlled resonance frequency, or vanishing, which will mitigate dephasing.

#### A. No-tip influence distance

To establish to what extent the magnetic field induced by the tip affects the measurements, we must know how the resonance frequency, given in Eq. (3) behaves as a function of tip-sample distance when we experiment with different STM tips.

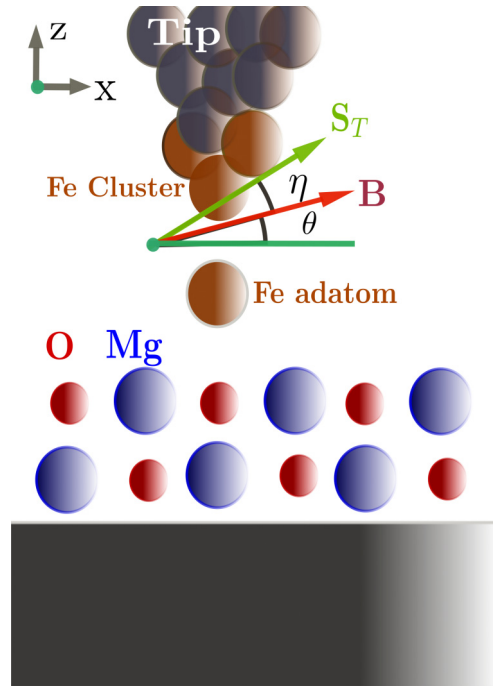


FIG. 1. Sketch of a Fe atom in MgO/Ag and an SPSTM tip.

The influence of the tip arises from the  $z$  component of the total magnetic field term [see Eq. (9)]. It is important to note that  $\mathcal{F}$  is small and therefore, in most situations, we can usually assume that  $\Delta \simeq 4\mu_B g_z B_{\text{eff}}(z)$ . In Fig. 2, we depict the ESR frequency as a function of the tip-adatom distance for different values of the tip anisotropy,  $\eta$  (see Fig. 1). In solid lines, we show the corresponding calculations obtained by direct diagonalization of our multi-orbital electronic model (see Appendix A) for two different experimental situations. Filled dots in Fig. 2 show calculations performed using the perturbative expression Eq. (3). Panel (a) corresponds to an external magnetic field almost in-plane [6–8,10–13] while in panel (b) an out-of-plane external magnetic field is applied [35]. Expectedly, the resonance frequency goes to a plateaulike regime for a large atom-tip distance, as both exchange and dipolar interactions fade away.

Interestingly, we observe in Fig. 2 a point at which all the curves intersect at a value approximately given by  $4\mu_B g_z B_z$ , independent of the dipolar and exchange field of the tip. This happens when the off-plane component of the tip field vanishes,  $B_{\text{tip}}^{(z)} = 0$  [see Eqs. (4) and (9)]. Using the expressions for the dipolar and exchange fields we obtain an implicit equation for the tip-atom distance  $z_n$  for which these two contributions cancel each other:

$$J_0 e^{-z_n/l_0} = \frac{g^z \gamma_t M_{\text{tip}}}{z_n^3}, \quad (14)$$

where  $\gamma_t = \mu_B \mu_0 / 4\pi$ . The NOTIN distance  $z_n$  depends on the voltage through the  $g$ -factor as shown Eq. (11). For the choice of  $J_0, l_0, M_{\text{tip}}$  and  $V_{\text{DC}} = 0$ , we find the NOTIN point at  $z_n^{(0)} = 0.59 \text{ nm}$ . The super index in  $z_n$  indicates that the calculations were performed with no external electric field. As shown in the last equation and in Fig. 2, this value remains independent of both the orientation and magnitude of the external magnetic

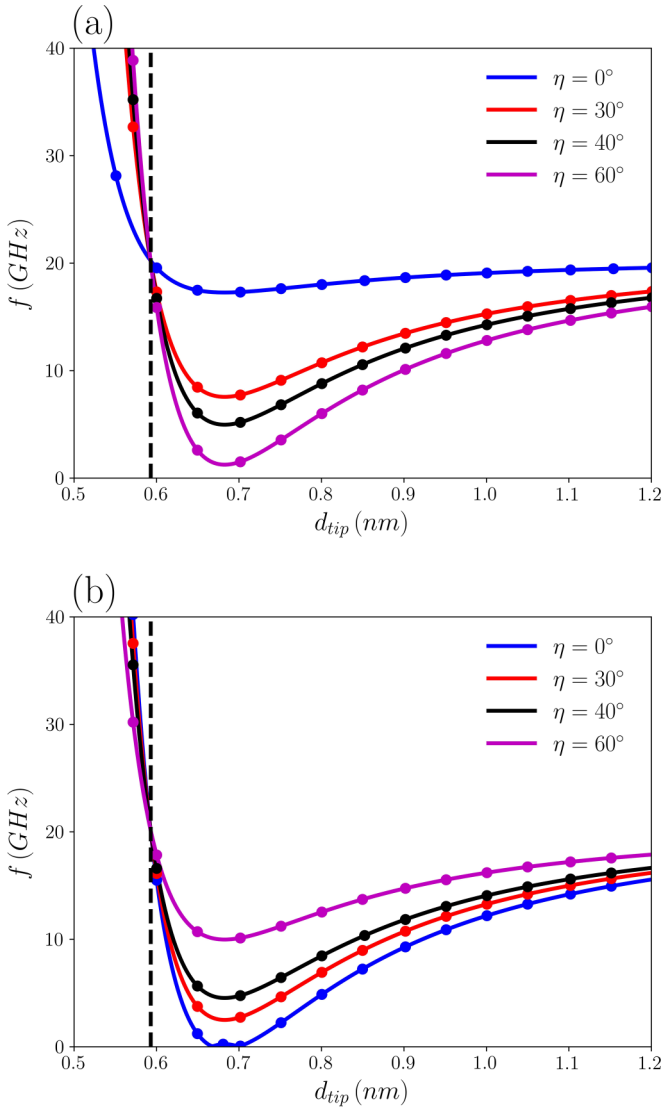


FIG. 2. Resonance frequency as a function of the tip atom distance for different values of the tip anisotropy  $\eta$  and  $V_{DC} = 0$  mV. (a) shows results for  $\theta = 8^\circ$  and  $B_{ext} = 0.9$  T. (b) corresponds to the results with  $\theta = 90^\circ$  and  $B_{ext} = 0.1$  T. Solid lines show results obtained by direct diagonalization of the multiorbital model while dots represent perturbative results obtained using Eq. (3).

field. Equation (14) allows the NOTIN distance to be related to the parameters that describe the behavior of the tip and the adatom. The dependence of this particular point on the surface atom is through  $g$ , whereas the influence of the tip comes through  $J_0$ ,  $M_{tip}$ , and  $l_0$ . Figure 3 shows the position where the field of the tip is zero as a function of the parameters that define the tip. It is clear from Fig. 3 and Eq. (14), as we should expect, that for exchange-only tips ( $M_{tip} = 0$ ) or dipolar-only tips ( $J_0 = 0$ ), there is no NOTIN distance. It is also clear from the figure that for a wide range of the parameter  $J_0^*$  ( $J_0^* > 0.5$  meV) the variations in the parameters do not have a great influence on the position of the NOTIN. It is important to note, as shown in Fig. 3(b), that the results obtained using Eq. (14) are in complete agreement with the results obtained by the direct diagonalization of the multiorbital model.

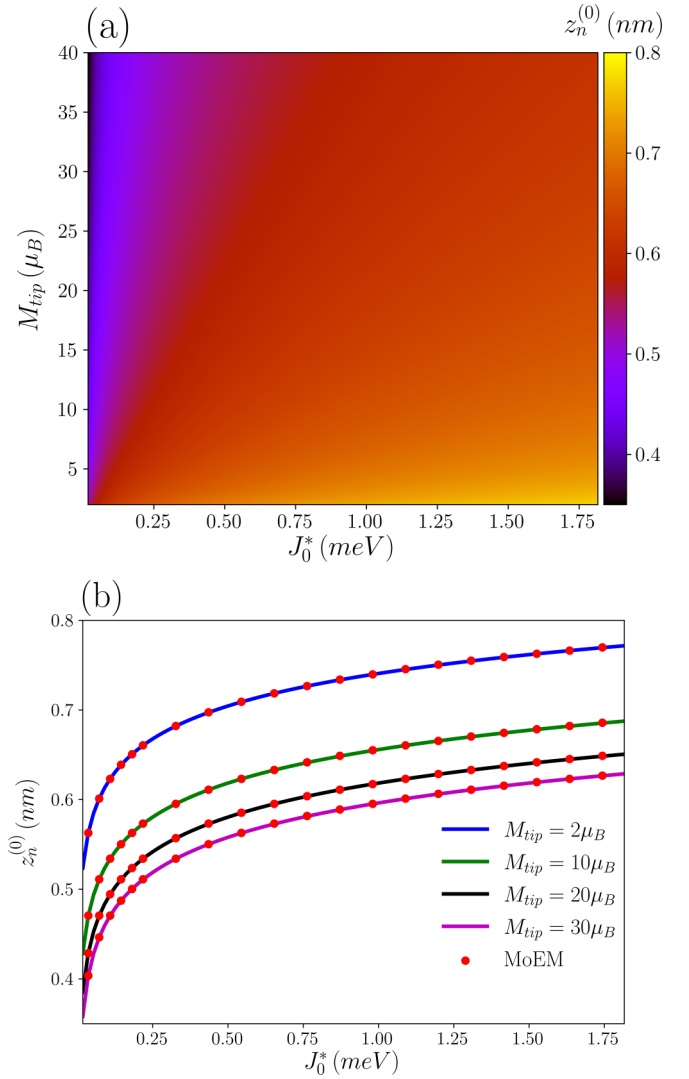


FIG. 3. Notin distance as a function of the tip parameters  $J_0^*$  and  $M_{tip}$ . (a) Contour map of the NOTIN distance (for  $V_{DC} = 0$  mV) as a function of the exchange coupling between the tip and the surface atom  $J_0^*$  and the magnetic moment of the tip  $M_{tip}$ . (b) NOTIN distance  $z_n^{(0)}$  as a function of  $J_0^*$  for four different values of  $M_{tip}$ . Filled dots show calculations with the multiorbital electronic model and continuous lines show calculations using Eq. (14).

We observe, for the parameters employed in Fig. 2, that displacements of 10 pm from the NOTIN point produce tip magnetic fields of 50 mT. Although the NOTIN position seems to be optimal to carry out most of the measurements, it is clear that any small tip drift or tip vibration can make the scenario a little more complex by inducing unwanted magnetic fields and unexpected frequency alterations. For instance, the NOTIN distance has a small dependence on  $V_{DC}$ , by virtue of the piezoelectric displacement of the surface atom and the modulation of its  $g$  factor, given in Eq. (11). For the chosen value of tip parameters and up  $V_{DC} = 200$  mV, we obtain changes around 1 pm or less in the NOTIN tip position.

### B. Control of the $V_{DC}$ dependence

We now analyze how the DC electric field of the tip changes the resonance frequency of the surface spin. This

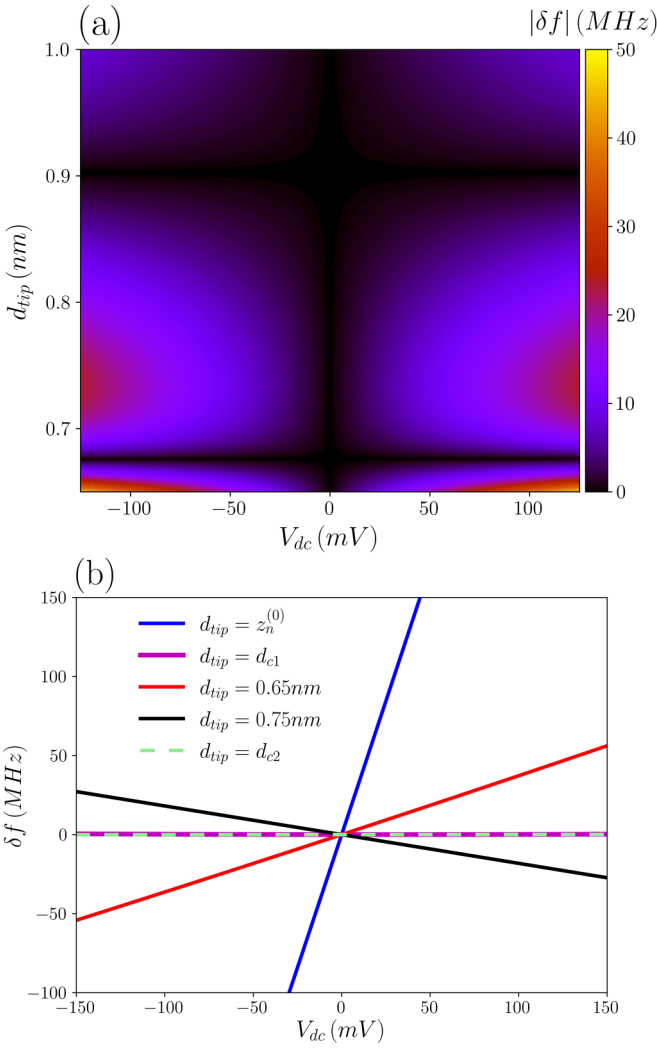


FIG. 4. Shift of the resonance frequency versus  $V_{DC}$  [Eq. (15)]. (a) Contour map of  $|\delta f|$  as a function of the tip atom distance and external voltage for  $\eta = 60^\circ$  and  $B = 0.9$  T almost in-plane ( $\theta = 8^\circ$ ). In (b), we plot the shift  $\delta f$  (a horizontal section of the map) as a function of the external voltage for five different tip-atom distances.

dependence arises from the combination of the piezoelectric displacement of the surface atom [Eq. (10)] and the distance dependence of the frequency [Eq. (13)]. Depending on the target application, this dependence could be either a resource, for instance, to control  $f$  without modifying the applied magnetic field, or a problem to avoid, as it can bring additional dephasing, as discussed below. In order to quantify these matters, we define the variation of the resonant frequency  $f$  with respect to its  $V_{DC} = 0$  value,

$$\delta f = f(V_{DC}) - f(V_{DC} = 0). \quad (15)$$

The contour map of Fig. 4(a) shows  $|\delta f|$  [Eq. (15)] as a function of both the external voltage and the tip-atom distance, for  $\theta = 8^\circ$ ,  $\eta = 60^\circ$ , and  $B_{\text{ext}} = 0.9$  T. We focus our attention first on regions where  $\delta f$  is small. This happens both for  $d_{\text{tip}} \simeq 0.7$  nm and  $d_{\text{tip}} \simeq 0.9$  nm. In these two regions, we have  $df/dV_{DC} = 0$  [see Eq. (3)] at  $V_{DC} = 0$ .

We now discuss how a small value of  $df/dV_{DC}$  mitigates decoherence. It is known that, for a two-level system, stochastic fluctuations of fluctuating energy difference lead to pure dephasing. Specifically, let us write the effective field as the sum of the static contribution and a time-dependent fluctuation part,  $B_{\text{eff}}^z = B_{\text{eff},0}^z + b(t)$ . For the fluctuation function, we assume that the time average vanishes,  $\overline{b(t)} = 0$  but has nonvanishing short-memory fluctuations over time,  $\mathcal{S}_b(t) \equiv \overline{b(t)b(t+\tau)}$  that decay rapidly when  $t \gg \tau$ , and have an amplitude that scale with  $b_0^2$ . We define the Fourier transform  $k(\omega) \equiv \frac{1}{2} \int_{-\infty}^{\infty} b(t)b(t+\tau)e^{-i\omega t} dt$ . We thus see that the stochastic field is characterized by the amplitude  $b_0$  and a correlation time  $\tau$ . We can write down the decoherence rate as [42]

$$\frac{1}{T_2} = \frac{(2g^z\mu_B)^2}{\hbar} k(0) \propto \frac{(2g^z\mu_B)^2}{\hbar} b_0^2 \tau. \quad (16)$$

We note this dephasing mechanism is independent of the current-induced dephasing that has been observed experimentally [7] and would act even if no current is tunneling through the surface spin. Now, it is apparent both electrical noise in  $V_{DC}$ ,  $\delta V_{DC}(t)$ , and mechanical noise in  $\delta z(t)$  will contribute to the amplitude of the fluctuations of the effective field:

$$b(t) = \frac{\partial B_{\text{eff}}^z}{\partial z} \left( \frac{\partial z}{\partial V_{DC}} \delta V_{DC}(t) + \delta z(t) \right) \quad (17)$$

and thereby to dephasing. Equation (17) describes the stochastic fluctuations of the effective magnetic field acting on the surface spin,  $b(t)$ , related to the tip-adatom distance-dependent interaction. These are driven by two independent mechanisms: first, voltage noise, that in turn produces piezoelectric displacements of the adatom; second, mechanical noise of the adatom. Given that, according to Eq. (16)  $T_2^{-1} \propto b_0^2$ , and in turn, the amplitude of the fluctuations satisfies  $b_0 \propto \delta f$ , the regions in Fig. 4 where  $\delta f$  is small imply reduced decoherence due to electric and mechanical noise.

Importantly, since the ESR-STM driving of Fe on MgO is associated with the in-plane component of the effective field [29] and the frequency is dominated by the off-plane component, it is possible to have a vanishing  $df/dz$ , and at the same time a large Rabi coupling.

Let us consider how the regions where  $df/dV_{DC}$  is not small so that the DC bias could be used to achieve electrical control of the resonance frequency. In Fig. 4(b), we plot the change as a function of applied external voltage for five particular tip-atom distances. For  $d_{c1} \simeq 0.67$  nm (violet line) and  $d_{c2} \simeq 0.9$  nm (cyan dashed line) we retrieve the stable regions discussed above, for which  $f$  is independent of  $V_{DC}$ . In contrast, for the other three values of  $d_{\text{tip}}$  we find a strong dependence of  $f$  on  $V_{DC}$ . We draw attention to the immense value of  $df/dV_{DC}$  at the NOTIN point.

#### IV. DETERMINATION OF TIP ANISOTROPY

So far, we have assumed that  $\eta$ , the misalignment angle between the tip magnetic moment and the external magnetic field, is unknown and can take values in a rather wide range, going from almost  $0^\circ$  up to  $60^\circ$  [11,35]. The origin of this misalignment is necessarily related to some type of tip

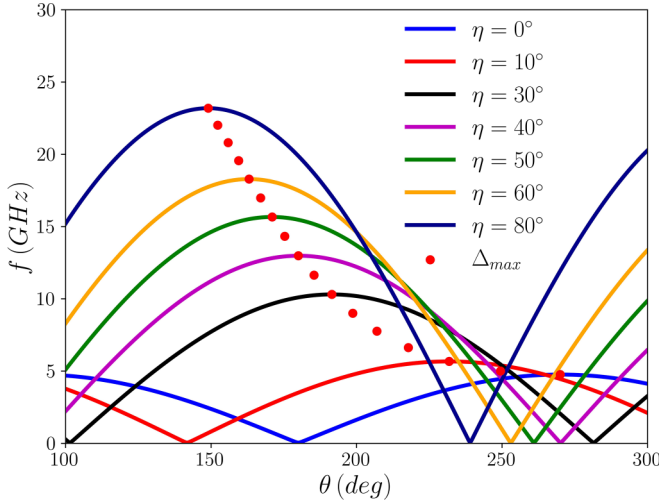


FIG. 5. Resonance frequency as a function of the external magnetic orientation,  $\theta$ , for different values of  $\eta$ . The calculation was performed by exact diagonalization of the few electron model (see Appendix A). All the calculations were performed for  $B = 0.1$  T and  $d_{\text{tip}} = 0.7$  nm.

magnetic anisotropy that can arise both from anisotropy in the  $g$  factor and single-ion anisotropies [11,29,32,35,43].

We now propose a simple experiment to determine  $\eta$ , similar to the one carried out by Kim *et al.* [44] to probe the magnetic anisotropy of hydrogenated Ti on the surface of MgO. Essentially, we propose to measure the resonant frequency for Fe on MgO as a function of the angle  $\theta$  formed between the external magnetic field and the surface, away from the NOTIN point. Our calculations (see Fig. 5) show a marked dependence of  $f$  on  $\theta$ , expected because the Fe atom is sensitive mostly to the  $z$  component of the effective field. We note how, for different values of  $\eta$ , our calculations show a lateral shift of the curves. Specifically, we find a dependence of the maximum as a function of the tip anisotropy  $\eta$ .

Imposing that the derivative of Eq. (3) with respect to  $\theta$  vanishes and using Eq. (9), we obtain the following implicit equation for  $\eta$ :

$$\tan(\theta_{\max}) = \frac{\varepsilon_{\text{ext}} + \varepsilon_{\text{tip}} \cos(\eta)}{\varepsilon_{\text{tip}} \sin(\eta)}. \quad (18)$$

where

$$\begin{aligned} \varepsilon_{\text{ext}} &= g^z \mu_B B, \\ \varepsilon_{\text{tip}} &= \varepsilon_{\text{exc}} - \varepsilon_{\text{dip}}, \\ \varepsilon_{\text{exc}} &= 2J_0 e^{-z/l_0}, \\ \varepsilon_{\text{dip}} &= 2\gamma_t \frac{g^z M_{\text{tip}}}{|z|^3}. \end{aligned} \quad (19)$$

Here,  $g_z$  is defined in Eq. (11) and  $z = d_{\text{tip}} - \delta z$ . Thus experimental determination of  $\theta_{\max}$  and the tip effective fields,  $\varepsilon_{\text{tip}}$  and  $\varepsilon_{\text{exc}}$ , permit to read out the value of  $\eta$ . Importantly, in the limit of a very small magnetic field, we have a simple linear relation between  $\eta$  and  $\theta_{\max}$ , independent of  $\varepsilon_{\text{tip}}$  and  $\varepsilon_{\text{exc}}$ ,

$$\eta = \frac{\pi}{2} - \theta_{\max}. \quad (20)$$

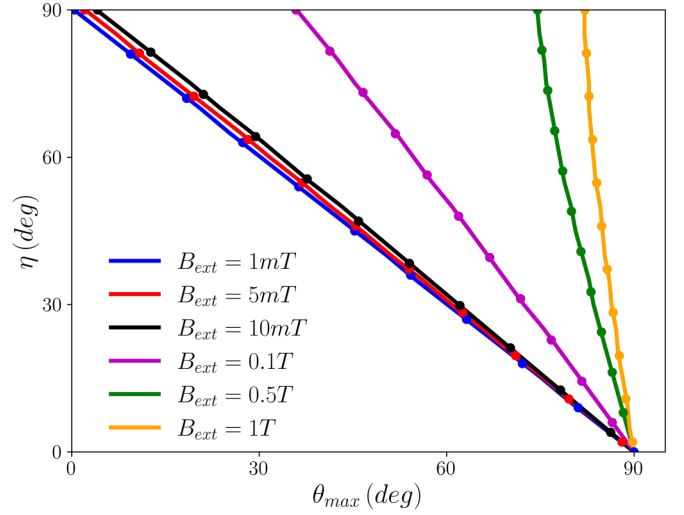


FIG. 6. Detuning angle  $\eta$  as a function of  $\theta_{\max}$  ( $d_{\text{tip}} = 0.7$  nm) obtained with two methods: solid lines show the results obtained from the exact diagonalization of the few electron model while dots show results obtained from the transcendental Eq. (18).

In Fig. 6, we plot the anisotropy angle  $\eta$  as a function of  $\theta_{\max}$  for different values of the external magnetic field. Solid lines and filled circles show an excellent agreement of the results obtained by numerical diagonalization of our multi-orbital model and the ones obtained from solving Eq. (18). It is clear from this figure that in the small magnetic field limit ( $B_{\text{ext}} \rightarrow 0$ ) all the curves converge to the expression in Eq. (20). This suggests that carrying out the experiments with small magnetic fields (it is even possible to carry them out at a vanishing field [13]) would make it possible to estimate the misalignment angle  $\eta$  without having to infer the values of  $\varepsilon_{\text{dip}}$  and  $\varepsilon_{\text{exc}}$ . We also note that, in this limit, the relation between  $\eta$  and  $\theta_{\max}$  is independent of  $V_{\text{DC}}$ , which should simplify the experiment.

## V. SUMMARY AND CONCLUSIONS

In this work, we have studied the interactions between an STM tip and a single Fe atom on a MgO surface, relevant for single spin ESR-STM experiments [3,7]. The tip influences the surface spin via three different mechanisms: dipolar coupling, exchange interactions, and the electric coupling that induces piezoelectric displacements of the Fe ion, modulating both its spin interactions with the tip as well as its  $g$  factor and crystal field parameters. All these interactions produce shifts of the Fe energy levels and a modification of the resonance frequency  $f$ . Therefore, in order to use the surface spin as a sensor for magnetometry, it is important to assess the tip contributions.

The main implications of our results for future experimental work are the following.

(1) We have provided a theoretical basis for the existence of a sweet spot at which the dipolar and exchange spin couplings cancel each other, the so-called NOTIN point. In figure 2 we have calculated the NOTIN point for  $V_{\text{DC}} = 0$ . We have then discussed the influence of  $V_{\text{DC}}$  on the resonance frequency  $f$  and the NOTIN point.

(2) We have calculated a phase diagram for the stability of  $f$  with respect to variations in  $V_{\text{DC}}$  as a function of both tip-atom distance  $d_{\text{tip}}$  and  $V_{\text{DC}}$ . We stress that two different regimes may be of practical interest. First, the regions in this phase diagram where the frequency is very stable with respect to voltage fluctuations. We have discussed how in this region decoherence due to both mechanical and electrical noise would be mitigated. Second, regions in which large variations of the resonant frequency can be obtained by changing  $V_{\text{DC}}$ . Whereas this would increase decoherence it would permit an electrical control of the resonant frequency that may be convenient in some situations.

(3) We have proposed an experimental protocol to measure  $\eta$ , the misalignment angle between the tip magnetization and the external magnetic field. The protocol is based on measuring  $f(\theta)$ , where  $\theta$  is the orientation of the applied field. We have shown that the maxima of this curve depend on  $\eta$  and in the limit of vanishing external field, this relation is straightforward: these angles,  $\theta$  and  $\eta$ , are dephased by  $90^\circ$  [see Eq. (20)].

We hope that all of these results may help the design of future ESR-STM experiments, especially in cases where accurate magnetometry is required [45,46]. In this work, we have focused on the case of Fe adatoms on MgO. Similar results should be obtained in the case of other ESR-STM active adatoms, such as Ti-H on MgO, with quantitative modification arising from the differences of  $g$  factor anisotropies and magnetic moments between these systems.

### ACKNOWLEDGMENTS

A.F. acknowledges ANPCyT (PICT2019-0654). A.F., S.S.G., and S.A.R. acknowledge CONICET (PUE22920170100089CO and PIP11220200100170) and partial financial support from UNNE. J.F.R. acknowledges financial support from FCT (Grant No. PTDC/FIS-MAC/2045/2021), FEDER /Junta de Andalucía, (Grant No. P18-FR-4834), Generalitat Valenciana funding Prometeo2021/017 and MFA/2022/045, and funding from MICIIN-Spain (Grant No. PID2019-109539GB-C41).

### APPENDIX A: MULTIORBITAL ELECTRONIC MODEL

We start with the Hamiltonian for the 6 electrons in the  $d$  levels of Fe:

$$\mathcal{H}_{\text{Fe}} = H_{\text{CF}} + H_{\text{SO}} + H_Z + H_{ee} + H_{\text{Tip}}, \quad (\text{A1})$$

where  $H_{\text{CF}}$  is the crystal field Hamiltonian,  $H_{\text{SO}}$  is the spin-orbit coupling,  $H_Z$  is the Zeeman Hamiltonian,  $H_{ee}$  is the Coulomb term, and  $H_{\text{Tip}}$  accounts for the interaction of the atom with the tip. The crystal field part of the Hamiltonian is obtained from the representation of the DFT Hamiltonian in the basis of maximally localized Wannier orbitals [29,38,47,48]

$$H_{\text{CF}} = \frac{1}{2} \sum_{m,m',\sigma} \langle m | h_{\text{CF}} | m' \rangle d_{m\sigma}^\dagger d_{m'\sigma}, \quad (\text{A2})$$

where  $d_{m\sigma}^\dagger$  ( $d_{m\sigma}$ ) denotes the creation (annihilation) operator of an electron with spin  $\sigma$  in the  $\ell = 2$ ,  $\ell_z = m$  state of the Fe atom, denoted by  $\phi_m(\vec{r})$ , assumed to be equal to the product

of a radial hydrogenic function (with effective charge  $Z$  and a effective Bohr radius  $a_\mu$ ) and a spherical harmonic. The one-particle elements are calculated from [29]

$$h_{\text{CF}} = D l_z^2 + F (l_x^4 + l_y^4), \quad (\text{A3})$$

where  $D = -290$  meV and  $F = -10$  meV are crystal field parameters obtained from DFT calculations and wannierization [29,32]. We add the spin-orbit coupling operator [29,38,48]

$$H_{\text{SO}} = \lambda_{\text{SO}} \sum_{mm',\sigma\sigma'} \langle m\sigma | \vec{\ell} \cdot \vec{S} | m'\sigma' \rangle d_{m\sigma}^\dagger d_{m'\sigma'}, \quad (\text{A4})$$

where we take  $\lambda_{\text{SO}} = 35$  meV [29,38]. Zeeman Hamiltonian reads

$$H_Z = \mu_B \vec{B} \cdot \sum_{mm',\sigma\sigma'} \langle m, \sigma | (\vec{l} + g\vec{S}) | m'\sigma' \rangle d_{m\sigma}^\dagger d_{m'\sigma'}, \quad (\text{A5})$$

where  $g = 2$ . The Coulomb term reads

$$H_{ee} = \frac{1}{2} \sum_{\substack{m,m' \\ n,n'}} V_{mm'n'n'} \sum_{\sigma\sigma'} d_{m\sigma}^\dagger d_{n\sigma'}^\dagger d_{n'\sigma'} d_{m'\sigma}. \quad (\text{A6})$$

For the evaluation of the Coulomb integrals  $V_{mm'n'n'}$ , we transform the angular part to a basis of eigenstates of  $l = 2$ . In the basis of eigenstates of  $l = 2$ , all the Coulomb integrals scale linearly with the value of  $V_{0000} = U$  [38,48]. Here we take, as in previous works,  $U = 5.0$  eV [29,38]. Now, to end with an adequate description of the situation, we need to describe the interaction of the atom with the tip. Along this work, we consider exchange and dipolar interaction  $H_{\text{tip}} = H_{\text{ex}} + H_{\text{dip}}$ . We can write the exchange interaction as  $J_{\text{ex}}(z) \vec{S}_{\text{tip}} \cdot \vec{S}$  [29] where  $S_{\text{tip}}$  is the total spin of the spin-polarized tip and  $J_{\text{ex}}$  is the exchange coupling between the surface spin and the tip. The exchange coupling depends exponentially on the tip-adatom distance and it can be written [29]

$$J_{\text{ex}}(z) = J_0 e^{-z/l_0}. \quad (\text{A7})$$

where  $J_0$  and  $l_0$  depend on the tip and the adatom. We ignore the quantum fluctuations of the magnetic moment of the apex atom or atoms, quenched by the combination of an applied magnetic field and strong Korringa damping with the tip electron bath [49]. Therefore we treat the tip spin in a mean-field or classical approximation, following Refs. [29,50], and replace  $S_{\text{tip}}$  by its statistical average  $\langle S_{\text{tip}} \rangle$ . Then, the tip-atom exchange interaction contribution to the Hamiltonian reads

$$H_{\text{ex}} = J_{\text{ex}} \langle \vec{S}_{\text{tip}} \rangle \cdot \sum_{mm',\sigma\sigma'} \langle m, \sigma | \vec{S} | m'\sigma' \rangle d_{m\sigma}^\dagger d_{m'\sigma'}, \quad (\text{A8})$$

where  $\langle \vec{S}_{\text{tip}} \rangle = \langle S_{\text{tip}} \rangle \hat{n}_T$  and  $\hat{n}_T = (\cos(\theta + \eta), 0, \sin(\theta + \eta))$  (see Fig. 1).

The dipolar interaction between the magnetic moment of the tip and the surface spin, where the tip creates a magnetic field whose orientation depends on the tip characteristics, gives us a dipolar term of the form

$$H_{\text{dip}} = \mu_B \vec{B}_{\text{dip}} \cdot \sum_{mm',\sigma\sigma'} \langle m, \sigma | (\vec{l} + g\vec{S}) | m'\sigma' \rangle d_{m\sigma}^\dagger d_{m'\sigma'}, \quad (\text{A9})$$

where the effective magnetic field created by the tip is defined in Eq. (8).

The few-body Hamiltonian Eq. (A1) is solved exactly, by numerical diagonalization in a space constructed with all the states that accommodate six electrons in five spin-degenerate  $d$  orbitals.

### APPENDIX B: EFFECTIVE SPIN MODEL

The lowest energy manifold of the Hamiltonian defined in the previous section has five states separated from the rest of the spectra. These states correspond to a ground state with  $S = 2$  result of accommodating six electrons in 5  $d$  orbitals and can be described in terms of a simple effective spin model [32,38]:

$$\hat{H}_{\text{eff}} = -\mathcal{D}_2 \hat{S}_z^2 + \mathcal{D}_4 \hat{S}_z^4 - \mathcal{F}(\hat{S}_+^4 + \hat{S}_-^4) + \mathcal{H}_1, \quad (\text{B1})$$

where the spin operators act on the  $S = 2$  subspace. The term  $\mathcal{H}_1$  accounts for the interaction of the adatom with the tip and the external field [see Eqs. (4) and (2)]. The anisotropy terms  $\mathcal{D}_2$ ,  $\mathcal{D}_4$ , and  $\mathcal{F}$  can be obtained from the diagonalization of Hamiltonian Eq. (A1) with no magnetic field and no tip. We obtain  $\mathcal{D}_2 = 4.86$  meV,  $\mathcal{D}_4 = 0.23$  meV, and  $\mathcal{F} = 4.06$  neV. Now, the spectrum of the ground state manifold has an ESR active space formed by a doublet of states with  $S_z = \pm 2$ . Yet, this doublet has a zero-field splitting (ZFS), given by  $\Delta = 48\mathcal{F} = 0.2$   $\mu\text{eV}$ , due to quantum spin tunneling [39–41].

Our model for the Fe atom at MgO taking into account the interaction of the surface spin with the magnetic moment of the tip, described by Hamiltonian (A1), can be solved by numerical diagonalization. We can calculate the resonance frequency  $f = \Delta/h = (E_1 - E_0)/h$  as a function of the tip-atom distance  $z = d_{\text{tip}}$  for different values of  $J_0$  and  $M_{\text{tip}}$ . Comparing with experimentally determined parameters and the resonance frequency curves obtained experimentally [7,8,12,13,18,34,35], in particular paying attention to the results presented in Refs. [12,34,35], a reasonable set of values are  $l_0 = 0.04\text{--}0.06$  nm,  $J_0 = 10\text{--}60$  eV ( $J_0^* = 0.5\text{--}3$  meV), and  $M_{\text{tip}} = 10\mu_B\text{--}40\mu_B$ .

#### Perturbative expressions

The eigenvalues of the effective spin Hamiltonian assuming  $B_{\text{eff}}^{(x)} = 0$  can be written

$$\begin{aligned} E_4 &= 0, \\ E_3 &= -\mathcal{D}_2 + \mathcal{D}_4 + g^z \mu_B B_{\text{eff}}^z, \\ E_2 &= -\mathcal{D}_2 + \mathcal{D}_4 - g^z \mu_B B_{\text{eff}}^z, \\ E_1 &= -4\mathcal{D}_2 + 16\mathcal{D}_4 + \sqrt{(24\mathcal{F})^2 + (2g^z \mu_B B_{\text{eff}}^z)^2}, \\ E_0 &= -4\mathcal{D}_2 + 16\mathcal{D}_4 - \sqrt{(24\mathcal{F})^2 + (2g^z \mu_B B_{\text{eff}}^z)^2}, \end{aligned} \quad (\text{B2})$$

and the eigenvectors

$$\begin{aligned} |4\rangle &= |S_z = 0\rangle, \\ |3\rangle &= |S_z = 1\rangle, \\ |2\rangle &= |S_z = -1\rangle, \end{aligned}$$

$$\begin{aligned} |1\rangle &= C_1^1 |S_z = 2\rangle + C_2^1 |S_z = -2\rangle, \\ |0\rangle &= C_1^0 |S_z = 2\rangle + C_2^0 |S_z = -2\rangle, \end{aligned} \quad (\text{B3})$$

where  $\{|S_z = i\rangle\}$  are eigenstates of  $S_z$  for  $S = 2$ . We introduce  $B_{\text{eff}}^x$  as a perturbation. Using perturbation up to second order in  $B_{\text{eff}}^x$ , we have that

$$E_i^{(2)} = E_i^{(0)} + (\mu_B g^x B_{\text{eff}}^x)^2 \sum_{m \neq i} \frac{|\langle m | \hat{S}_x | i \rangle|^2}{E_i^{(0)} - E_m^{(0)}}. \quad (\text{B4})$$

Assuming  $B_{\text{eff}} \ll \mathcal{D}_i$  with  $i = 2$  and 4, we obtain

$$E_i^{(2)} = E_i^{(0)} + \frac{3}{2} \frac{(\mu_B g^x B_{\text{eff}}^x)^2}{E_i^{(0)} - E_3^{(0)}}. \quad (\text{B5})$$

We thus see that, in the subspace of the two lowest energy states of the Fe adatom, the effect of  $B_x$  is negligible, to linear order in  $B_x$ , and finally we can write the gap of the system as follows:

$$\Delta \approx 2\sqrt{(24\mathcal{F})^2 + (2\mu_B g^z B_{\text{eff}}^z)^2}. \quad (\text{B6})$$

As the anisotropy terms, we obtain the  $g$  tensor from the diagonalization of Hamiltonian Eq. (A1). For the values quoted above and ignoring the effect of the tip, we get  $g_z = 2.8$ .

### APPENDIX C: EFFECT OF THE EXTERNAL ELECTRIC FIELD ON THE HAMILTONIAN PARAMETERS

Our model assumes a piezoelectric distortion of the atom-tip distance due to the external electric field. This distortion modulates crystal field parameters in the Hamiltonian Eq. (A1):

$$\begin{aligned} F &= F_{eq} + \left. \frac{dF}{dz} \right|_{z_{eq}} \delta z, \\ D &= D_{eq} + \left. \frac{dD}{dz} \right|_{z_{eq}} \delta z, \end{aligned} \quad (\text{C1})$$

and tip terms directly by their dependency with  $\delta z$  through  $z = d_{\text{tip}} - \delta z$ , where  $d_{\text{tip}}$  is the tip-atom distance at the equilibrium. Here we take, using DFT calculations [29],  $\left. \frac{dF}{dz} \right|_{z_{eq}} = 280 \frac{\text{meV}}{\text{nm}}$  and  $\left. \frac{dD}{dz} \right|_{z_{eq}} = 0$ .

For the effective spin Hamiltonian, Eqs. (B1) and (1), we can calculate the modulation of the parameters by direct diagonalization of Eq. (A1) taking into account the modulation of

TABLE I. Parameters of the effective Hamiltonian and their modulations.

| $X$             | $X_{eq}$ | $\alpha_X$                       |
|-----------------|----------|----------------------------------|
| $\mathcal{D}_2$ | 4.9 meV  | 134 $\mu\text{eV}/\text{pm}$     |
| $\mathcal{D}_4$ | 0.2 meV  | 14 $\mu\text{eV}/\text{pm}$      |
| $\mathcal{F}$   | 4.1 neV  | -0.0002 $\mu\text{eV}/\text{pm}$ |
| $g^x$           | 2.0      | -0.36 $\text{nm}^{-1}$           |
| $g^z$           | 2.8      | 9.02 $\text{nm}^{-1}$            |

the crystal field parameters described above:

$$\begin{aligned}
 \mathcal{D}_2 &= \mathcal{D}_{2_{eq}} + \alpha_{\mathcal{D}_2} \delta z, \\
 \mathcal{D}_4 &= \mathcal{D}_{4_{eq}} + \alpha_{\mathcal{D}_4} \delta z, \\
 \mathcal{F} &= \mathcal{F}_{eq} + \alpha_{\mathcal{F}} \delta z, \\
 g^x &= g_{eq}^x + \alpha_{g^x} \delta z, \\
 g^z &= g_{eq}^z + \alpha_{g^z} \delta z
 \end{aligned}
 \tag{C2}$$

with

$$\alpha_X = \left. \frac{\partial X}{\partial F} \frac{\partial F}{\partial z} \right|_{z_{eq}} + \left. \frac{\partial X}{\partial D} \frac{\partial D}{\partial z} \right|_{z_{eq}}.
 \tag{C3}$$

Finally, calculated modulation and equilibrium parameters for the effective Hamiltonian are depicted in Table I.

- 
- [1] Y. Manassen, R. J. Hamers, J. E. Demuth, and A. J. Castellano Jr, Direct Observation of the Precession of Individual Paramagnetic Spins on Oxidized Silicon Surfaces, *Phys. Rev. Lett.* **62**, 2531 (1989).
- [2] A. V. Balatsky, M. Nishijima, and Y. Manassen, Electron spin resonance-scanning tunneling microscopy, *Adv. Phys.* **61**, 117 (2012).
- [3] S. Baumann, W. Paul, T. Choi, C. P. Lutz, A. Ardavan, and A. J. Heinrich, Electron paramagnetic resonance of individual atoms on a surface, *Science* **350**, 417 (2015).
- [4] F. D. Natterer, K. Yang, W. Paul, P. Willke, T. Choi, T. Greber, A. J. Heinrich, and C. P. Lutz, Reading and writing single-atom magnets, *Nature (London)* **543**, 226 (2017).
- [5] T. Choi, W. Paul, S. Rolf-Pissarczyk, A. J. Macdonald, F. D. Natterer, K. Yang, P. Willke, C. P. Lutz, and A. J. Heinrich, Atomic-scale sensing of the magnetic dipolar field from single atoms, *Nat. Nanotechnol.* **12**, 420 (2017).
- [6] K. Yang, Y. Bae, W. Paul, F. D. Natterer, P. Willke, J. L. Lado, A. Ferrón, T. Choi, J. Fernández-Rossier, A. J. Heinrich *et al.*, Engineering the Eigenstates of Coupled Spin-1/2 Atoms on a Surface, *Phys. Rev. Lett.* **119**, 227206 (2017).
- [7] P. Willke, W. Paul, F. D. Natterer, K. Yang, Y. Bae, T. Choi, J. Fernández-Rossier, A. J. Heinrich, and C. P. Lutz, Probing quantum coherence in single-atom electron spin resonance, *Sci. Adv.* **4**, eaaq1543 (2018).
- [8] P. Willke, Y. Bae, K. Yang, J. L. Lado, A. Ferrón, T. Choi, A. Ardavan, J. Fernández-Rossier, A. J. Heinrich, and C. P. Lutz, Hyperfine interaction of individual atoms on a surface, *Science* **362**, 336 (2018).
- [9] Y. Bae, K. Yang, P. Willke, T. Choi, A. J. Heinrich, and C. P. Lutz, Enhanced quantum coherence in exchange coupled spins via singlet-triplet transitions, *Sci. Adv.* **4**, eaau4159 (2018).
- [10] K. Yang, P. Willke, Y. Bae, A. Ferrón, J. L. Lado, A. Ardavan, J. Fernández-Rossier, A. J. Heinrich, and C. P. Lutz, Electrically controlled nuclear polarization of individual atoms, *Nat. Nanotechnol.* **13**, 1120 (2018).
- [11] K. Yang, W. Paul, F. D. Natterer, J. L. Lado, Y. Bae, P. Willke, T. Choi, A. Ferrón, J. Fernández-Rossier, A. J. Heinrich *et al.*, Tuning the Exchange Bias on a Single Atom from 1 mT to 10 T, *Phys. Rev. Lett.* **122**, 227203 (2019).
- [12] P. Willke, K. Yang, Y. Bae, A. J. Heinrich, and C. P. Lutz, Magnetic resonance imaging of single atoms on a surface, *Nat. Phys.* **15**, 1005 (2019).
- [13] P. Willke, A. Singha, X. Zhang, T. Esat, C. P. Lutz, A. J. Heinrich, and T. Choi, Tuning single-atom electron spin resonance in a vector magnetic field, *Nano Lett.* **19**, 8201 (2019).
- [14] W. M. van Weerdenburg, M. Steinbrecher, N. P. van Mullekom, J. W. Gerritsen, H. von Allwörden, F. D. Natterer, and A. A. Khajetoorians, A scanning tunneling microscope capable of electron spin resonance and pump-probe spectroscopy at mk temperature and in vector magnetic field, *Rev. Sci. Instrum.* **92**, 033906 (2021).
- [15] M. Steinbrecher, W. M. J. Van Weerdenburg, E. F. Walraven, N. P. E. Van Mullekom, J. W. Gerritsen, F. D. Natterer, D. I. Badrtdinov, A. N. Rudenko, V. V. Mazurenko, M. I. Katsnelson, A. van der Avoird, G. C. Groenenboom, and A. A. Khajetoorians, Quantifying the interplay between fine structure and geometry of an individual molecule on a surface, *Phys. Rev. B* **103**, 155405 (2021).
- [16] F. D. Natterer, F. Patthey, T. Bilgeri, P. R. Forrester, N. Weiss, and H. Brune, Upgrade of a low-temperature scanning tunneling microscope for electron-spin resonance, *Rev. Sci. Instrum.* **90**, 013706 (2019).
- [17] J. Hwang, D. Krylov, R. Elbertse, S. Yoon, T. Ahn, J. Oh, L. Fang, W.-j. Jang, F. H. Cho, A. J. Heinrich *et al.*, Development of a scanning tunneling microscope for variable temperature electron spin resonance, *Rev. Sci. Instrum.* **93**, 093703 (2022).
- [18] T. S. Seifert, S. Kovarik, C. Nistor, L. Persichetti, S. Stepanow, and P. Gambardella, Single-atom electron paramagnetic resonance in a scanning tunneling microscope driven by a radio-frequency antenna at 4 k, *Phys. Rev. Res.* **2**, 013032 (2020).
- [19] P. Kot, M. Ismail, R. Drost, J. Siebrecht, H. Huang, and C. R. Ast, Electric control of spin transitions at the atomic scale, *arXiv:2209.10969*.
- [20] L. M. Veldman, L. Farinacci, R. Rejali, R. Broekhoven, J. Gobeil, D. Coffey, M. Ternes, and A. F. Otte, Free coherent evolution of a coupled atomic spin system initialized by electron scattering, *Science* **372**, 964 (2021).
- [21] K. Yang, S.-H. Phark, Y. Bae, T. Esat, P. Willke, A. Ardavan, A. J. Heinrich, and C. P. Lutz, Probing resonating valence bond states in artificial quantum magnets, *Nat. Commun.* **12**, 993 (2021).
- [22] S. Kovarik, R. Robles, R. Schlitz, T. S. Seifert, N. Lorente, P. Gambardella, and S. Stepanow, Electron paramagnetic resonance of alkali metal atoms and dimers on ultrathin mgo, *Nano Lett.* **22**, 4176 (2022).
- [23] P. Willke, T. Bilgeri, X. Zhang, Y. Wang, C. Wolf, H. Aubin, A. Heinrich, and T. Choi, Coherent spin control of single molecules on a surface, *ACS Nano* **15**, 17959 (2021).
- [24] X. Zhang, C. Wolf, Y. Wang, H. Aubin, T. Bilgeri, P. Willke, A. J. Heinrich, and T. Choi, Electron spin resonance of single iron phthalocyanine molecules and role of their non-localized spins in magnetic interactions, *Nat. Chem.* **14**, 59 (2022).

- [25] L. Farinacci, L. M. Veldman, P. Willke, and S. Otte, Experimental determination of a single atom ground state orbital through hyperfine anisotropy, *Nano Lett.* **22**, 8470 (2022).
- [26] K. Yang, W. Paul, S.-H. Phark, P. Willke, Y. Bae, T. Choi, T. Esat, A. Ardavan, A. J. Heinrich, and C. P. Lutz, Coherent spin manipulation of individual atoms on a surface, *Science* **366**, 509 (2019).
- [27] A. Caso, B. Horowitz, and L. Arrachea, Model for electron spin resonance in stm noise, *Phys. Rev. B* **89**, 075412 (2014).
- [28] P. Berggren and J. Fransson, Electron paramagnetic resonance of single magnetic moment on a surface, *Sci. Rep.* **6**, 25584 (2016).
- [29] J. L. Lado, A. Ferrón, and J. Fernández-Rossier, Exchange mechanism for electron paramagnetic resonance of individual adatoms, *Phys. Rev. B* **96**, 205420 (2017).
- [30] A. M. Shakirov, A. N. Rubtsov, and P. Ribeiro, Spin transfer torque induced paramagnetic resonance, *Phys. Rev. B* **99**, 054434 (2019).
- [31] J. R. Gálvez, C. Wolf, F. Delgado, and N. Lorente, Co-tunneling mechanism for all-electrical electron spin resonance of single adsorbed atoms, *Phys. Rev. B* **100**, 035411 (2019).
- [32] A. Ferrón, S. A. Rodríguez, S. S. Gómez, J. L. Lado, and J. Fernández-Rossier, Single spin resonance driven by electric modulation of the g-factor anisotropy, *Phys. Rev. Res.* **1**, 033185 (2019).
- [33] F. Delgado and N. Lorente, A theoretical review on the single-impurity electron spin resonance on surfaces, *Prog. Surf. Sci.* **96**, 100625 (2021).
- [34] T. S. Seifert, S. Kovarik, P. Gambardella, and S. Stepanow, Accurate measurement of atomic magnetic moments by minimizing the tip magnetic field in stm-based electron paramagnetic resonance, *Phys. Rev. Res.* **3**, 043185 (2021).
- [35] T. S. Seifert, S. Kovarik, D. M. Juraschek, N. A. Spaldin, P. Gambardella, and S. Stepanow, Longitudinal and transverse electron paramagnetic resonance in a scanning tunneling microscope, *Sci. Adv.* **6**, eabc5511 (2020).
- [36] A. Abragam and B. Bleaney, *Electron Paramagnetic Resonance of Transition Ions* (Oxford University Press, Oxford, 1970).
- [37] S. Baumann, F. Donati, S. Stepanow, S. Rusponi, W. Paul, S. Gangopadhyay, I. G. Rau, G. E. Pacchioni, L. Gragnaniello, M. Pivetta, J. Dreiser, C. Piamonteze, C. P. Lutz, R. M. Macfarlane, B. A. Jones, P. Gambardella, A. J. Heinrich, and H. Brune, Origin of Perpendicular Magnetic Anisotropy and Large Orbital Moment in Fe Atoms on MgO, *Phys. Rev. Lett.* **115**, 237202 (2015).
- [38] A. Ferrón, J. L. Lado, and J. Fernández-Rossier, Electronic properties of transition metal atoms on Cu<sub>2</sub>N/Cu(100), *Phys. Rev. B* **92**, 174407 (2015).
- [39] M. J. Klein, On a degeneracy theorem of kramers, *Am. J. Phys.* **20**, 65 (1952).
- [40] A. Garg, Topologically quenched tunnel splitting in spin systems without kramers' degeneracy, *Europhys. Lett.* **22**, 205 (1993).
- [41] F. Delgado, S. Loth, M. Zielinski, and J. Fernández-Rossier, The emergence of classical behaviour in magnetic adatoms, *Europhys. Lett.* **109**, 57001 (2015).
- [42] F. Delgado and J. Fernández-Rossier, Spin decoherence of magnetic atoms on surfaces, *Prog. Surf. Sci.* **92**, 40 (2017).
- [43] M. dos Santos Dias, B. Schweglinghaus, S. Blügel, and S. Lounis, Relativistic dynamical spin excitations of magnetic adatoms, *Phys. Rev. B* **91**, 075405 (2015).
- [44] J. Kim, W.-J. Jang, T. H. Bui, D.-J. Choi, C. Wolf, F. Delgado, Y. Chen, D. Krylov, S. Lee, S. Yoon, C. P. Lutz, A. J. Heinrich, and Y. Bae, Spin resonance amplitude and frequency of a single atom on a surface in a vector magnetic field, *Phys. Rev. B* **104**, 174408 (2021).
- [45] Y. del Castillo and J. Fernández-Rossier, Certifying entanglement of spins on surfaces using esr-stm, [arXiv:2211.14205](https://arxiv.org/abs/2211.14205).
- [46] N. Karjalainen, Z. Lippo, G. Chen, R. Koch, A. O. Fumega, and J. L. Lado, Hamiltonian inference from dynamical excitations in spin quantum dots, [arXiv:2212.07893](https://arxiv.org/abs/2212.07893).
- [47] N. Marzari, A. A. Mostofi, J. R. Yates, I. Souza, and D. Vanderbilt, Maximally localized wannier functions: Theory and applications, *Rev. Mod. Phys.* **84**, 1419 (2012).
- [48] A. Ferrón, F. Delgado, and J. Fernández-Rossier, Derivation of the spin hamiltonians for fe in mgo, *New J. Phys.* **17**, 033020 (2015).
- [49] F. Delgado, C. Hirjibehedin, and J. Fernández-Rossier, Consequences of kondo exchange on quantum spins, *Surf. Sci.* **630**, 337 (2014).
- [50] S. Yan, D.-J. Choi, J. A. Burgess, S. Rolf-Pissarczyk, and S. Loth, Control of quantum magnets by atomic exchange bias, *Nat. Nanotechnol.* **10**, 40 (2015).